Inorganic Chemistry

Article

pubs.acs.org/IC

# Magnetic Structure and Properties of the $Na_2CoP_2O_7$ Pyrophosphate Cathode for Sodium-Ion Batteries: A Supersuperexchange-Driven Non-Collinear Antiferromagnet

Prabeer Barpanda,[†,∥,*] Maxim Avdeev,[‡,∥] Chris D. Ling, Jiechen Lu,[†] and Atsuo Yamada[†,▽]

[†]Department of Chemical System Engineering, The University of Tokyo, 7-3-1 Hongo, Bunkyo-ku, Tokyo 113-8656, Japan

[‡]Bragg Institute, B87, Australian Nuclear Science and Technology Organisation, Locked Bag 2001, Kirrawee DC NSW 2232, Australia

[§]School of Chemistry, The University of Sydney, Sydney, NSW 2006, Australia

[▽]Unit of Elements Strategy Initiative for Catalysts & Batteries, ESICB, Kyoto University, Kyoto 615-8510, Japan

**ABSTRACT:** The crystal and magnetic structure and properties of the $Na_2CoP_2O_7$ $Na^+$-ion battery cathode material have been characterized by magnetic susceptibility, specific heat, and variable-temperature neutron powder diffraction measurements. $Na_2CoP_2O_7$ crystallizes in the orthorhombic space group $Pna2_1$ with $a$ = 15.4061(3) Å, $b$ = 10.28854(9) Å, and $c$ = 7.70316(15) Å, having a layered structure with slabs of $[CoP_2O_7]_\infty$ separated by Na cations. The magnetic property measurements and neutron diffraction data analysis reveal that the material undergoes long-range ordering to a noncollinear antiferromagnetic G-type structure below $T_N \approx 6.5$ K. The magnetic structure is rationalized as a result of supersuperexchange between $Co^{2+}$ atoms linked by phosphate groups.

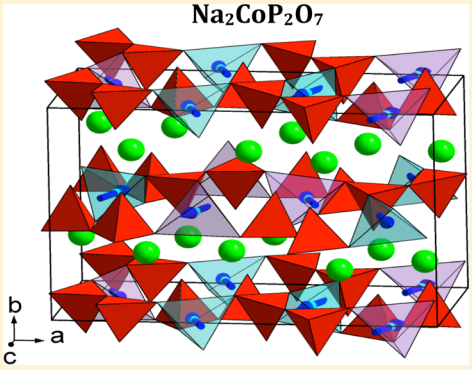


## INTRODUCTION

Combating the demand for mobile energy supply to empower portable consumer electronics and (plug-in hybrid) electric vehicles, various electrochemical energy storage devices have been widely explored, Li-ion batteries being at the forefront.[1,2] The last two decades' effort, triggered by commercialization of the $LiCoO_2$−graphite battery by the Sony Corporation in 1991, has led to the exploration and commercialization of various transition-metal oxide cathodes (e.g., $LiMn_2O_4$, $LiMn_{3/2}Ni_{1/2}O_4$, $LiCo_{1/3}Mn_{1/3}Ni_{1/3}O_2$) along with a myriad of polyanionic compounds.[3,4] With the advent of olivine $LiFePO_4$ in 1997,[5] electrochemists have tried and tested families of polyanionic cathodes such as borates ($LiMBO_3$), silicates ($Li_2MSiO_4$), fluorophosphates ($LiMPO_4F$) and fluorosulfates ($LiMSO_4F$), etc.[6−10] Although many such systems have formidable electrochemical performance, they suffer from low kinetics, inconvenient synthesis, atmospheric poisoning, and/or low redox voltage. From an applications point of view, the $PO_4$-based systems are the most suitable cathodes, because of their robust structure, ease of synthesis, economy, and good thermal/chemical stability.

Besides olivine $LiMPO_4$, the alkali-metal pyrophosphates ($A_2MP_2O_7$, where A = Li or Na, and M = transition metals) form a diphosphate ($P_2O_7$, i.e., $PO_4$−$PO_4$) family of compounds showing rich structural diversity and the widest range of redox potential (2.0−4.9 V).[11] Over the last 15 years, numerous lithium-based pyrophosphate compounds, $Li_{2-x}MP_2O_7$ (where $x$ = 0−1, and M = Fe, Co, Mn, Ni, V, Ti), have been reported as potential cathode materials.[12−16] In contrast, there has been no report on electrochemical activity of any sodium-based pyrophosphate ($Na_2MP_2O_7$) cathode compound, although they have been investigated by crystallographers for over four decades.[11] With the current renewed interest in Na-ion batteries for economic large-scale energy storage systems, inorganic chemists have tried to unravel new Na-based oxide and polyanionic insertion compounds.[17] Putting the pyrophosphate framework compounds on anvil, we have recently discovered two novel (3.0 V) electrochemically active sodium-based cathodes: $Na_2CoP_2O_7$ and $Na_2FeP_2O_7$.[18,19]

Although these pyrophosphate oxyanionic compounds have been intensely studied, with a focus on their ionic and electrochemical properties, there is also a dearth of detailed analyses of their magnetic properties. Fundamental investigation of the magnetic structure of cathode compounds can reveal interesting physical phenomena, such as magneto-electric effects, geometric frustration, noncollinearity, and magneto-dielectric coupling.[20] As a first step in our effort to investigate a series of $PO_4$-based cathode materials, here, we report the magnetic structure and physical properties of $Na_2CoP_2O_7$ cathode compound. $Na_2CoP_2O_7$ forms an interesting system, showing structural complexity and distinct polymorphism, namely, a three-dimensional (3D) framework (pink form) and layered (blue form) systems.[21−23] We have probed the magnetic structural analysis of the layered-$Na_2CoP_2O_7$ with a

**Received:** October 8, 2012
**Published:** December 17, 2012

close ensemble of $CoO_4$ tetrahedra. Using temperature-dependent magnetic susceptibility, we have observed a very low magnetic transition temperature (6.5 K). Furthermore, employing neutron powder diffraction study, we propose a G-type noncollinear antiferromagnetic Co-spin configuration.

## EXPERIMENTAL SECTION

**Material Synthesis.** The $Na_2CoP_2O_7$ powder sample was synthesized via conventional solid-state synthesis, using a stoichiometric 2:1 molar mixture of $NaH_2PO_4$ (Wako, 99%) and $CoC_2O_4$ (Kojundo, 99+%). These precursors were intimately mixed by wet planetary ball-milling in acetone media for 1 h (600 rpm), employing Cr-hardened stainless steel (Cr-SS) milling media and container. After drying out the acetone, the precursor mixture was ground in an agate mortar, pelletized, and sintered at 600 °C (heating rate = 10 °C/min) for 6 h in a tubular furnace under a steady argon flow to obtain the desired phase.

**Structural Analysis.** High-precision powder X-ray diffraction (XRD) analysis was performed on polycrystalline $Na_2CoP_2O_7$, using a Bruker AXS D8 ADVANCE diffractometer (operating at 35 mA, 40 kV) equipped with a Co K$\alpha$ source ($\lambda_1$ = 1.78897 Å, $\lambda_2$ = 1.7929 Å) and a Vantec-1 linear position-sensitive detector. The scan was performed in the 2$\theta$ range of 10°−70° (at steps of 0.5° min$^{-1}$). The XRD data analysis confirmed complete formation of the desired phase with no impurity and an orthorhombic structure (space group No. 33, $Pna2_1$).

**Magnetic Susceptibility and Specific Heat Measurement.** Magnetic susceptibility and heat capacity measurements of $Na_2CoP_2O_7$ were conducted employing a Quantum Design PPMS instrument. The susceptibility was recorded in field-cooled (FC) and zero-field-cooled (ZFC) modes in an applied field of 50 kOe over the temperature range of 2−300 K. Magnetization data as a function of field were collected up to ±100 kOe at 2 K. Heat capacity measurements were performed on a $Na_2CoP_2O_7$ pellet over the temperature range of 2−50 K.

**Neutron Powder Diffraction.** Neutron powder diffraction (NPD) data were collected on the high-resolution powder diffractometer Echidna at the OPAL facility (Lucas Height, Australia), using neutrons with a wavelength of 2.4395 Å. The high intensity of Echidna offers excellent resolution at low angles, enabling the magnetic structure determination. For the measurements, a powder sample with a mass of ∼2 g was loaded into a 6-mm-diameter cylindrical vanadium can, and data were collected between 300 K and 3 K, using a closed-cycle refrigerator. Rietveld analysis[24] for magnetic structure determination was conducted using the FullProf[25] suite with the default neutron scattering lengths and $Co^{2+}$ magnetic form factors.

## RESULTS AND DISCUSSION

**Crystal Structure.** $Na_2CoP_2O_7$ has been reported to exist in three distinct polymorphs: triclinic ($P1$), orthorhombic ($Pna2_1$), and tetragonal ($P4_2/mnm$) phases.[21−23] While the triclinic phase is thermodynamically most unstable, both tetragonal and orthorhombic polymorphs, having similar structure, have been proposed as the most thermodynamically stable phases. However, our extensive synthetic investigation produced only the orthorhombic polymorph in every case, independent of the sintering temperature (500−800 °C), heating rate (1−10 °C min$^{-1}$), and annealing time (1−24 h). This polymorph is a layered structure with layers of mixed Co and P tetrahedral (i.e., $CoO_4$ and $PO_4$) units forming $[Co(P_2O_7)]^{2-}$ slabs parallel to (001), which are stacked with alternating layers of Na atoms (Figure 1). The Co species are linked to four oxygen atoms in tetrahedral fashion, one each from four surrounding $PO_4$ units, with an average Co−O bond length of 1.98(2) Å. When viewed along the (010) direction, the distinct organization of Na and Co channels is evident with

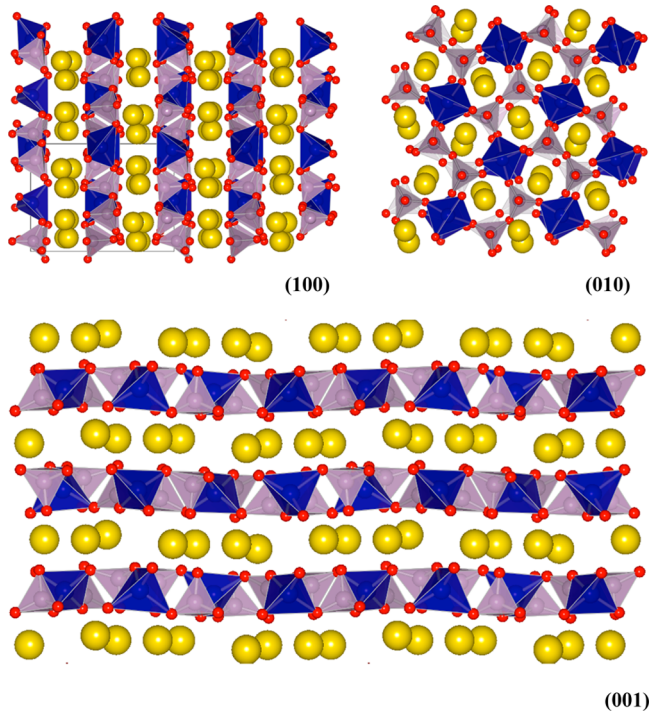


**Figure 1.** Schematic presentation of layer-structured orthorhombic polymorph of $Na_2CoP_2O_7$ viewed along the (100), (010), and (001) planes. The $CoO_4$ tetrahedra (blue), $PO_4$ tetrahedra (light gray), and Na atoms (yellow) are illustrated.

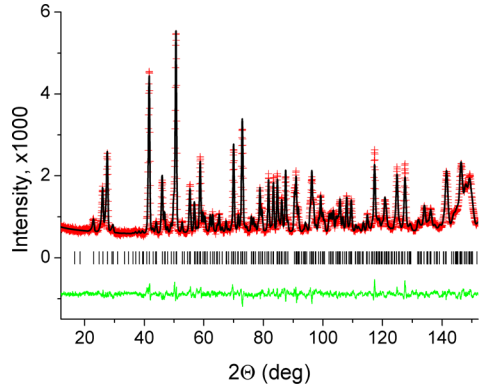


**Figure 2.** Rietveld plot for the $Na_2CoP_2O_7$ neutron powder diffraction (NPD) data at 300 K. The red crosses, black solid lines, and green solid lines indicate the observed and calculated curves and their difference, respectively. The black tick marks indicate the position of the diffraction peaks. $R_p$ = 4.00%, $R_{wp}$ = 5.06%, $R_{Bragg}$ = 4.71%, $\chi^2$ = 2.58.

each Co channel being surrounded by four Na channels. This layered compound presents continuous channels for $Na^+$-cation movement, responsible for the efficient Na (de)intercalation properties discovered recently.[19]

Note that the orthorhombic $Pna2_1$ modification of $Na_2CoP_2O_7$ is only a slightly distorted version of the tetragonal $P4_2/mnm$ form and can be related to the latter via the cell axes transformation ($2b,c,a$) and origin shift by ($x \approx 0$, $^3/_4$, $^1/_4$). This fact has implications for the magnetic structure analysis, as discussed below, and also suggests that there may be a crystal structural displacive phase transition between the orthorhombic and tetragonal modifications at elevated temperature, which will be investigated in the near future. In addition, previous reports


dx.doi.org/10.1021/ic302191d | Inorg. Chem. 2013, 52, 395−401

**Table 1. Crystal Structural Parameter for $Na_2CoP_2O_7$ at 300 K Refined against Neutron Powder Diffraction (NPD) Data[a]**

| atom | *x* | *y* | *z* |
|---|---|---|---|
| Co1 | 0.129(3) | 0.507(4) | −0.529(6) |
| Co2 | 0.1231(17) | 0.012(3) | −0.552(6) |
| P1 | 0.1914(5) | 0.0679(7) | −0.9048(10) |
| P2 | 0.0607(5) | 0.0499(7) | −0.1914(10) |
| P3 | 0.0537(5) | 0.4658(7) | −0.1518(10) |
| P4 | 0.1947(5) | 0.4813(6) | −0.9039(11) |
| Na1 | 0.301(2) | 0.2624(19) | −0.706(3) |
| Na2 | −0.0623(20) | 0.2381(18) | −0.406(4) |
| Na3 | 0.2315(17) | 0.2852(17) | −0.231(4) |
| Na4 | 0.0122(13) | 0.239(2) | −0.874(3) |
| O1 | 0.1379(6) | 0.1023(10) | −0.0739(13) |
| O2 | 0.1374(9) | 0.1211(12) | −0.7541(16) |
| O3 | 0.2848(5) | 0.1099(13) | 0.094(2) |
| O4 | 0.1872(10) | −0.0771(7) | −0.888(2) |
| O5 | 0.0698(10) | −0.0952(7) | −0.183(2) |
| O6 | 0.0803(10) | 0.1205(15) | −0.3630(14) |
| O7 | −0.0163(6) | 0.1077(15) | −0.093(2) |
| O8 | 0.1070(6) | 0.4283(12) | −0.9875(12) |
| O9 | −0.0341(6) | 0.3989(15) | −0.139(2) |
| O10 | 0.0456(10) | 0.6092(8) | −0.159(2) |
| O11 | 0.0923(9) | 0.4044(18) | −0.3119(16) |
| O12 | 0.1880(11) | 0.4185(13) | −0.7271(13) |
| O13 | 0.2728(7) | 0.4212(13) | −0.9925(20) |
| O14 | 0.1947(10) | 0.6275(7) | −0.907(3) |

[a]Space group $Pna2_1$ (No. 33) with all the atoms in 4a(*x*,*y*,*z*) Wyckoff sites. Numbers in parentheses are standard deviations of the last significant digit. $a$ = 15.4061(3) Å, $b$ = 10.28854(9) Å, $c$ = 7.70316(15) Å, $V$ = 1221.00(3) Å$^3$, overall isotropic temperature factor $B$ = 0.76(5) Å$^2$.

of the tetragonal form of $Na_2CoP_2O_7$ at room temperature[21−23] suggest that the tetragonal form can probably be quenched or stabilized by deviations from the ideal stoichiometry.

The orthorhombic distortion of the unit cell, which is defined as $(a_{orth}/2 - c_{orth})/(a_{orth}/2 + c_{orth})$, is rather small: $7.1 \times 10^{-6}$ and $5.9 \times 10^{-5}$ at 300 K and 3 K, respectively. However, the analysis of the atomic coordinates in the orthorhombic structure, with respect to the positions in the undistorted (i.e., tetragonal) form indicates that the atomic displacements within the unit cell are very substantial. Such a quantitative analysis has been done in terms of amplitudes of symmetry-adapted distortion modes, using the ISODISTORT software.[26] The amplitude of the X1 distortion mode was found to be, by far, the largest (i.e., 2.8 Å, compared to those for three remaining modes (0.29 Å, 0.71 Å, and 0.71 Å for GM1+, GM2+, and GM5−, respectively) at 300 K. The main effect the X1 mode produces on the crystal structure is antiphase rotation of $[PO_4]$ tetrahedra in the adjacent $[CoP_2O_7]$ layers, reminiscent of antiphase octahedra tilting in perovskites. Unsurprisingly, O atoms experience the largest displacements from the ideal positions. The average displacements of Co, P, Na, and O atoms produced by the combination of all four distortion modes are 0.14, 0.22, 0.28, and 0.33 Å, with O2, O3,

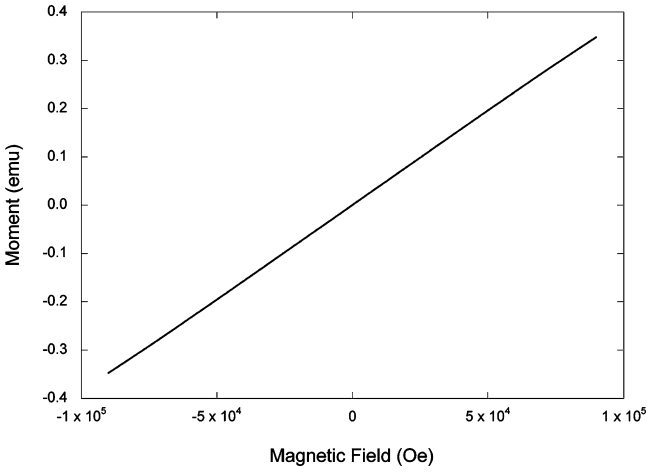


**Figure 4.** Magnetization as a function of field for $Na_2CoP_2O_7$ measured at 2 K.

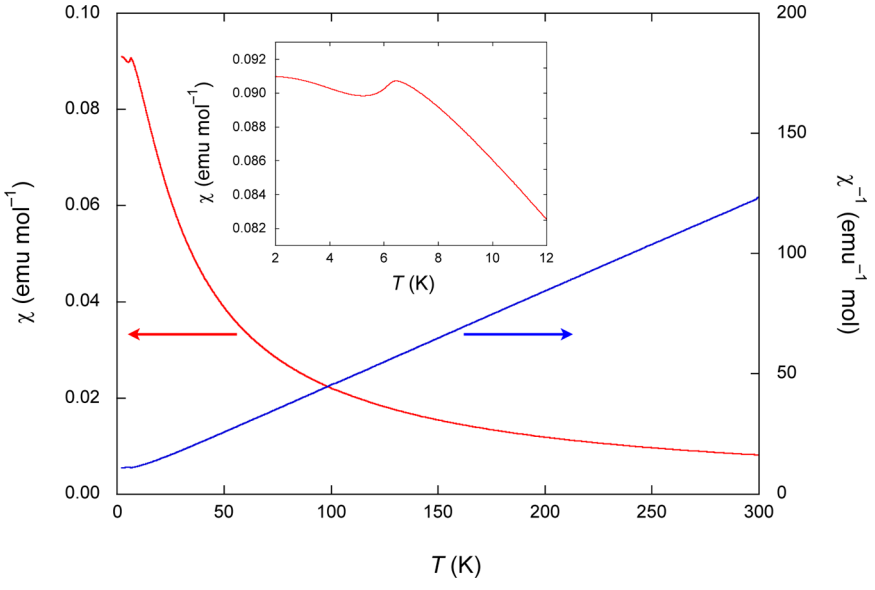


**Figure 3.** Magnetic susceptibility ($\chi$) and the corresponding $\chi^{-1}$ (inset) as a function of temperature for $Na_2CoP_2O_7$ measured with the applied field of $H$ = 50 kOe.


dx.doi.org/10.1021/ic302191d | *Inorg. Chem.* 2013, 52, 395−401

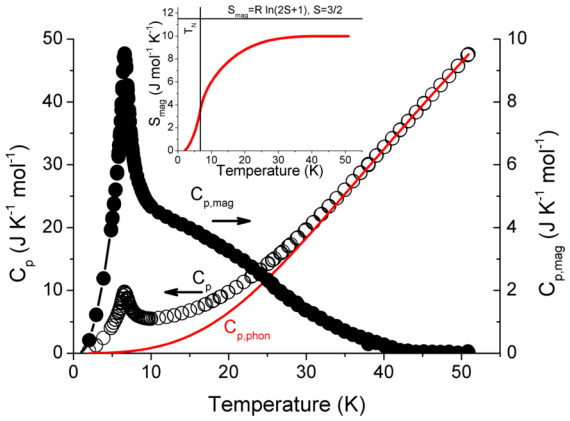


**Figure 5.** (Top) Total (open symbols) and magnetic specific heat (filled symbols) obtained by subtracting the lattice contribution (solid line) for $Na_2CoP_2O_7$. Inset shows magnetic entropy (solid line) obtained by integrating $C_{p,mag}/T$ vs $T$. The horizontal and vertical lines show the theoretical value for spin S = $^3/_2$ and ordering temperature, respectively.

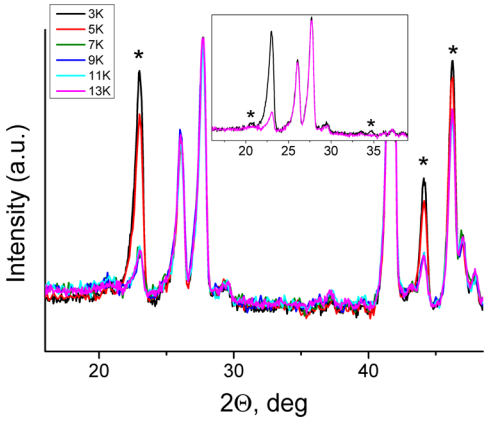


**Figure 6.** $Na_2CoP_2O_7$ NPD data collected in the vicinity of the magnetic phase transition. The peaks with additional intensity observed below 7 K are indicated with star symbols. The inset shows the enlarged region to illustrate the presence of the weak peaks corresponding to the Cx mode (see the text; the curve for 13 K has been offset for the sake of clarity).

**Table 2. Representational Analysis for the 4a($x,y,z$) Co1 and Co2 sites of the *Pna*2$_1$ Space Group and the Propagation Vector $k$ = [0,0,0]$^a$**

| IR | basis vectors | Shubnikov group |
|---|---|---|
| Γ1 | A$x$ G$y$ C$z$ | *Pna*2$_1$ |
| Γ2 | G$x$ A$y$ F$z$ | *Pn′a′*2$_1$ |
| Γ3 | C$x$ F$y$ A$z$ | *Pn′a*2$_1$′ |
| Γ4 | F$x$ C$y$ G$z$ | *Pna′*2$_1$′ |

$^a$The atomic positions are ($x,y,z$); ($-x,-y,z$ + $^1/_2$); ($x$ + $^1/_2$,$-y$ + $^1/_2$,$z$), ($-x$ + $^1/_2$,$y$ + $^1/_2$,$z$ + $^1/_2$). The ordering modes are defined as F(+ + + +), C(+ + − −), G(+ − + −), A(+ − − +).

O8, and O12 atoms displacing by as much as 0.47 Å, 0.46 Å, 0.54 Å, and 0.43 Å, respectively.

The final Rietveld fit to 300 K NPD data is presented in Figure 2, and the resulting crystallographic information is listed in Table 1.

**Magnetic Susceptibility and Specific Heat of $Na_2CoP_2O_7$.** The FC magnetic susceptibility $\chi$ and the

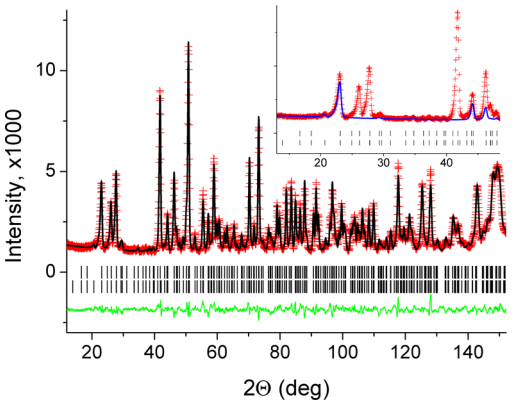


**Figure 7.** Rietveld plot for the $Na_2CoP_2O_7$ NPD data at 3 K. The red crosses, black solid lines, and green solid lines indicate the observed and calculated curves and their difference, respectively. The two rows of black tick marks indicate position of the nuclear (top) and magnetic (bottom) diffraction peaks. The blue curve in the inset shows magnetic contribution. $R_p$ = 4.29%, $R_{wp}$ = 5.46%, $R_{Bragg}$ = 4.36%, $\chi^2$ = 6.01, $R_{mag}$ = 6.69%.

corresponding $\chi^{-1}$, as a function of temperature for $Na_2CoP_2O_7$, are shown in Figure 3. No divergence between FC and ZFC data was observed. The $\chi$ plot reveals that the material undergoes a magnetic ordering transition at ∼6.5 K (Figure 3, inset). The susceptibility above 50 K follows the Curie−Weiss law with $\theta$ = −16.1 K and C = 2.56. The negative $\theta$ indicates predominantly antiferromagnetic (AFM) interactions between Co atoms. The plot of magnetization versus field plot at 2 K (Figure 4) is a perfect straight line with no hysteresis, as expected for a pure antiferromagnet; no evidence for a weak ferromagnetic component or canting of the AFM moments at low temperatures is observed. Probably due to the intrinsic anisotropy of $Co^{2+}$, no magnetic transition induced by the magnetic field up to 10T is detected. The effective magnetic moment $\mu_{eff}$ calculated from the Curie constant is 4.55 $\mu_B$, which exceeds the spin-only value of 3.87 $\mu_B$ expected for a $Co^{2+}$ ($d^7$) ion in high-spin (or any other) configuration. This is typical for divalent cobalt ($Co^{2+}$) ions, because of spin-orbit coupling, which allows a contribution from partially unquenched orbital angular momentum.

It may be interesting to compare the magnetic behavior of different polymorphs of $Na_2CoP_2O_7$. Although no magnetic data were reported for the triclinic "pink form",[21] the deviation of the magnetic susceptibility from the Curie−Weiss behavior previously observed for the "blue form" below 10 K was attributed to the onset of antiferromagnetic interactions in the $Co^{2+}$ sublattice.[22] Unfortunately, since the magnetic measurement was not complemented by a low-temperature crystal structural study, it is impossible to tell whether the sample was tetragonal or orthorhombic in the vicinity of 10 K. However, we do note that, in the subsequent electronic paramagnetic resonance (EPR) study of the "blue form" by the same authors,[23] tetragonal symmetry was found to be insufficient to explain the EPR data at low temperature and orthorhombic symmetry of $Co^{2+}$ sites was proposed as the origin of the observed complex spectrum.[23] This supports our results indicating that, at low temperature, a stable form of $Na_2CoP_2O_7$ is orthorhombic, which undergoes a magnetic transition at ∼6.5 K.

The specific heat data for $Na_2CoP_2O_7$ (Figure 5) shows a $\lambda$-type anomaly at ∼6.5 K, which is indicative of a long-range


dx.doi.org/10.1021/ic302191d | *Inorg. Chem.* 2013, 52, 395−401

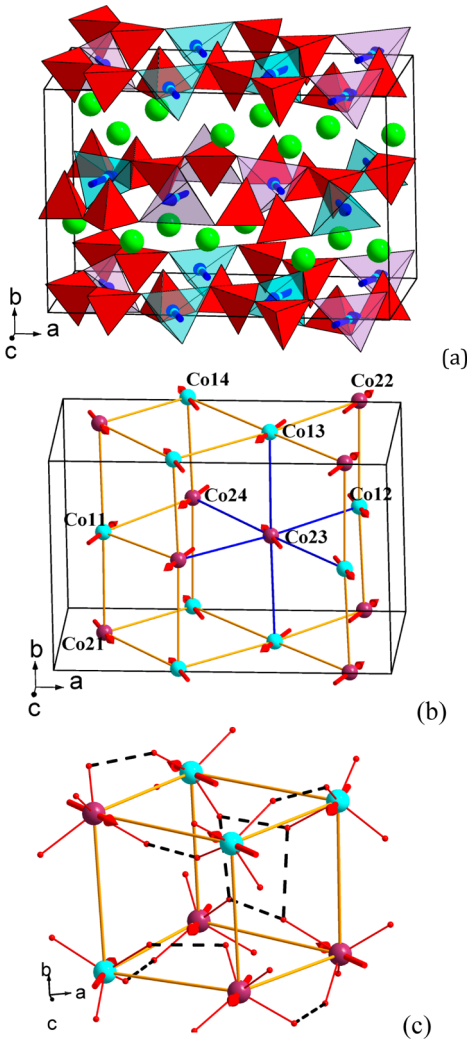


**Figure 8.** (a) General view of the magnetic structure of $Na_2CoP_2O_7$; (b) Co1 and Co2 sublattices with the atoms numbered in the order used for magnetic structure determination; the nearest coordination of one of the Co sites highlighted in blue indicates the closeness of the magnetic structure to the antiferromagnetic G-type; (c) super-superexchange paths between Co1 and Co2 sites, with the O$\mu$O contacts shorter than 3 Å shown as dashed lines.

magnetic ordering transition, in agreement with the magnetic susceptibility data. The magnetic contribution to heat capacity was obtained by subtracting the phonon contribution from the experimental data. Since no heat capacity data are available for a nonmagnetic analogue of $Na_2CoP_2O_7$, we estimated the lattice contribution using the Debye model:

$$c_{\mathrm{phon}}(T, \theta_{\mathrm{D}}) = 9R\left(\frac{T}{\theta_{\mathrm{D}}}\right)^3 \int_0^{\theta_{\mathrm{D}}/T} \frac{x^4 e^x}{(e^x - 1)^2}\, dx$$

where $R$ is the gas constant and $\theta_{\mathrm{D}}$ is the Debye temperature.

Furthermore, to account for the significant difference in atomic masses of the elements constituting $Na_2CoP_2O_7$, the experimental data were analyzed using a model with two-phonon spectra $c_{\mathrm{phon}} = 3c_{\mathrm{phon},1}(T,\theta_{\mathrm{D},1}) + 9c_{\mathrm{phon},2}(T,\theta_{\mathrm{D},2})$, with the first and second terms corresponding to Co/P and Na/O contributions, respectively. The fit (Figure 5) to the high-temperature range of the experimental data ($T$ > 40 K) yielded $\theta_{\mathrm{D},1}$ = 654 K and $\theta_{\mathrm{D},2}$ = 196 K, which is consistent with the lighter-element sublattice having the higher Debye temperature. As can be also seen in Figure 5, a nonzero $C_{\mathrm{p,mag}}$ signal appears at temperatures significantly above the $\lambda$-type anomaly. The overall shape of the magnetic heat capacity curve in combination with the negative $\theta_{\mathrm{CW}}$ suggest that $Na_2CoP_2O_7$ is a three-dimensional (3D) antiferromagnetic Heisenberg system with weakly coupled planes.[27] Although the variation in Co−Co distances due to low symmetry of the crystal structure made it impossible to extract values of magnetic exchange parameters, this was further corroborated by the results of the neutron diffraction data analysis.

Finally, the magnetic entropy was calculated as $S_{\mathrm{mag}} = \int_0^T C_{p,\mathrm{mag}}/T\, dT$ with $C_{p,\mathrm{mag}}$ extrapolated between the lowest measured temperature (2 K) and 0 K as $C_{p,\mathrm{mag}} = \alpha T^3$, assuming a spin-wave model for a 3D antiferromagnet.[28] The total magnetic entropy saturates at a value of 10 J mol$^{-1}$ K$^{-1}$, which is consistent with the theoretical value $S_{\mathrm{mag}} = R\ln(2S + 1)$ = 11.5 J mol$^{-1}$ K$^{-1}$ for $Co^{2+}$ in the S = $^3/_2$ spin state. Note that only approximately one-third of the total entropy is gained at $T_{\mathrm{N}}$, which also suggests that the $\lambda$-type anomaly at 6.5 K is associated with 3D ordering, whereas at higher temperature, the magnetic entropy is associated with short-range two-dimensional (2D) correlations.

**Table 3. Crystal Structural Parameter for $Na_2CoP_2O_7$ at 3 K Refined against NPD Data[a]**

| atom | $x$ | $y$ | $z$ |
|---|---|---|---|
| Co1 | 0.132(2) | 0.507(4) | −0.524(5) |
| Co2 | 0.1262(13) | 0.014(3) | −0.565(4) |
| P1 | 0.1902(5) | 0.0709(6) | −0.9080(10) |
| P2 | 0.0611(5) | 0.0526(7) | −0.1962(9) |
| P3 | 0.0542(5) | 0.4646(7) | −0.1488(10) |
| P4 | 0.1956(5) | 0.4798(6) | −0.9037(10) |
| Na1 | 0.301(2) | 0.2714(18) | −0.703(3) |
| Na2 | −0.0616(18) | 0.2335(17) | −0.402(4) |
| Na3 | 0.2305(16) | 0.2821(16) | −0.237(3) |
| Na4 | 0.0108(12) | 0.2408(20) | −0.876(3) |
| O1 | 0.1393(6) | 0.1037(9) | −0.0809(12) |
| O2 | 0.1350(8) | 0.1228(11) | −0.7576(14) |
| O3 | 0.2826(5) | 0.1121(12) | 0.100(2) |
| O4 | 0.1837(9) | −0.0768(7) | −0.8905(18) |
| O5 | 0.0731(9) | −0.0928(7) | −0.186(2) |
| O6 | 0.0757(9) | 0.1224(13) | −0.3714(12) |
| O7 | −0.0129(6) | 0.1096(13) | −0.0873(18) |
| O8 | 0.1068(5) | 0.4267(12) | −0.9833(11) |
| O9 | −0.0333(6) | 0.3937(13) | −0.1359(19) |
| O10 | 0.0433(9) | 0.6090(8) | −0.157(2) |
| O11 | 0.0929(8) | 0.4078(16) | −0.3122(14) |
| O12 | 0.1892(10) | 0.4233(12) | −0.7218(12) |
| O13 | 0.2717(7) | 0.4163(12) | −0.9966(18) |
| O14 | 0.1941(9) | 0.6279(7) | −0.908(2) |

[a]Space group $Pna2_1$ (No. 33) with all the atoms in 4a($x$,$y$,$z$) Wyckoff sites. Numbers in parentheses are standard deviations of the last significant digit. $a$ = 15.3758(2) Å, $b$ = 10.23927(8) Å, $c$ = 7.68699(11) Å, $V$ = 1210.22(3) Å$^3$, overall isotropic temperature factor $B$ = 0.01(4) Å$^2$.

**Magnetic Structure from Neutron Powder Diffraction Measurements.** The magnetic susceptibility and heat capacity data suggest a long-range magnetic transition at ~6.5 K. Indeed, examination of the neutron diffraction data collected at 3, 5, 7, 9, 11, 13, and 300 K reveals additional intensity, presumably due to antiferromagnetic ordering, developing below 7 K (see


dx.doi.org/10.1021/ic302191d | Inorg. Chem. 2013, 52, 395−401

Figure 6). All diffraction peaks with magnetic scattering contributions could be indexed to the crystallographic unit cell, i.e., with the propagation vector $k$ = (0,0,0). For the two Co 4$a$($x$,$y$,$z$) Wyckoff sites of the $Pna2_1$ space group, the magnetic representation decomposes in terms of four 1D irreducible representations (IR) as Γ = 3Γ1 + 3Γ2 + 3Γ3 + 3Γ7. The associated basis vectors are listed in Table 2.

Preliminary analysis indicated that the Γ1 and Γ3 IRs provide the best agreement with the experimental NPD data, with A$x$ and A$z$ being the primary ordering modes, respectively. Careful examination of the data also revealed much weaker magnetic peaks, corresponding to C$z$ and C$x$ modes, respectively (Figure 6), while no evidence of the modes defining the moment component along $y$-axis was found.

The fact that the Γ1 (A$x$, 0, C$z$) and Γ3 (C$x$, 0, A$z$) models produced similar agreement is not surprising, given the pseudo-tetragonal nature of the crystal structure. In the ideal tetragonal form, NPD data analysis would not have been able to distinguish the direction of the moment in the $a_{tetr}b_{tetr}$-plane. However, for the $Pna2_1$ orthorhombic modification, the displacements of Co atoms from their ideal positions are apparently sufficient for the NPD data analysis to favor the Γ3 (C$x$, 0, A$z$) model based on the $R_{mag}$ factor (6.69% vs 7.68% for the Γ1 (A$x$, 0, C$z$) model). Therefore, we used the Γ3 (C$x$, 0, A$z$) model, which is equivalent to the $Pn'a2_1'$ Shubnikov group in the previous discussion.

For refinements against the NPD data collected at 3 K, this model yielded magnetic moment components of 1.09(7), 0, and 2.71(3) $\mu$B along the $a_{orth}$, $b_{orth}$, and $c_{orth}$ axes, respectively, which translates to a total moment of 2.92(4)$\mu_B$; this value is very close to the spin-only value of 3 $\mu_B$ that is expected for the $3d^7$ configuration of $Co^{2+}$, and the canting angle from the $c$-axis in the $ac$-plane of 22(1)°. The final Rietveld plot and the magnetic structure are shown in Figures 7 and 8, respectively, with corresponding structural parameters listed in Table 3.

The magnetic structure can be well rationalized by considering the mutual arrangement of the metal sites and exchange paths. Despite the low symmetry and layered nature of the crystal structure, the $Co^{2+}$ atoms are located on a pseudo-cubic lattice with Co−Co distances in the range of 5.1−5.6 Å (see Figure 8b). In fact, the interlayer Co−Co distances are slightly shorter than the those within the $[CoP_2O_7]_\infty$ slabs.

Although the Co−O tetrahedra share neither edges nor corners, they are linked via the phosphate groups in the $ac$-plane that open Co−O···O−Co supersuperexchange paths with the large Co−O···O angles, favoring antiferromagnetic interactions (see Figure 8c). As a result, the material orders into a slightly noncollinear variation of antiferromagnetic G-type, as can be seen in Figure 8b, highlighting the nearest neighbors of one of the Co atoms. We find it especially significant that, despite similar interlayer and intralayer Co−Co distances, the shortest O···O distance between layers is substantially longer than the O···O distances within the $[CoP_2O_7]_\infty$ slabs (∼2.9 Å vs ∼2.5 Å, respectively). In fact, the former value is just above the van der Waals distance of 2.8 Å, which is considered to be a threshold for successful supersuperexchange via O···O contacts.[29] The implications of this difference in O···O intralayer and interlayer distances is consistent with the heat capacity data previously discussed; i.e., below ∼40 K, stronger supersuperexchange within $[CoP_2O_7]_\infty$ layers results in short-range 2D magnetic correlations and cooling to the much-lower temperature of 6.5 K is required to extend the interactions in the third dimension and establish a long-range 3D antiferromagnetic structure.

## CONCLUSIONS

In this article, we have reported the magnetic structure of the $Na_2CoP_2O_7$ sodium-ion cathode compound. The magnetic susceptibility follows a Curie−Weiss behavior above 50 K with $\theta$ = −16.1 K. Magnetic measurements reveal an antiferromagnetic ordering in $Na_2CoP_2O_7$ at $T_N$ = 6.5 K. The neutron powder diffraction (NPD) pattern at 3 K shows that the Co spins in each of the $[CoP_2O_7]_\infty$ layers are antiferromagnetically coupled and the Co spins in the adjacent $[CoP_2O_7]_\infty$ layers are arranged in a noncollinear manner.

## AUTHOR INFORMATION


### Corresponding Author

*Tel.: +81-3-5841-7295. Fax: +81-3-5841-7488. E-mail: prabeer@chemsys.t.u-tokyo.ac.jp.

### Author Contributions

‖These authors had equal contributions.


### Notes

The authors declare no competing financial interest.

## ACKNOWLEDGMENTS


The current work is partially supported by the "Element Strategy Initiative for Catalysts & Batteries" (ESICB) project by the Ministry of Education, Culture, Sports, Science and Technology, Japan (MEXT). P.B. acknowledges the Japan Society for the Promotion of Sciences for a JSPS Fellowship at the University of Tokyo. C.D.L.'s contribution was supported by the Australian Research Council (No. DP110102662). The crystal structure has been drawn using the VESTA software.[30]


## REFERENCES


(1) Goodenough, J. B.; Kim, Y. *Chem. Mater.* **2010**, *22*, 587−603.
(2) Etacheri, V.; Marom, R.; Elazari, R.; Salitra, G.; Aurbach, D. *Energy Environ. Sci.* **2011**, *4*, 3243−3262.
(3) Desilvestro, J.; Haas, O. *J. Electrochem. Soc.* **1990**, *137*, 5−22.
(4) Gong, Z.; Yang, Y. *Energy Environ. Sci.* **2011**, *4*, 3223−3242.
(5) Padhi, A. K.; Nanjundaswamy, K. S.; Goodenough, J. B. *J. Electrochem. Soc.* **1997**, *144*, 1188−1194.
(6) Yamada, A.; Iwane, N.; Harada, Y.; Nishimura, S.; Koyama, Y.; Tanaka, I. *Adv. Mater.* **2010**, *22*, 3583−3587.
(7) Nyten, A.; Abouimrane, A.; Armand, M.; Gustafsson, T.; Thomas, J. O. *Electrochem. Commun.* **2005**, *7*, 156−160.
(8) Ramesh, T. N.; Lee, K. T.; Ellis, B. E.; Nazar, L. F. *Electrochem. Solid-State Lett.* **2010**, *13*, 43−47.
(9) Recham, N.; Chotard, J. N.; Dupont, L.; Delacourt, C.; Walker, W.; Armand, M.; Tarascon, J. M. *Nat. Mater.* **2010**, *9*, 68−74.
(10) Barpanda, P.; Ati, M.; Melot, B. C.; Rousse, G.; Chotard, J. N.; Doublet, M. L.; Sougrati, M. T.; Corr, S. A.; Jumas, J. C.; Tarascon, J. M. *Nat. Mater.* **2011**, *10*, 772−779.
(11) Barpanda, P.; Nishimura, S.; Yamada, A. *Adv. Energy Mater.* **2012**, *2*, 841−859.
(12) Padhi, A. K.; Nanjundaswamy, K. S.; Masquelier, C.; Okada, S.; Goodenough, J. B. *J. Electrochem. Soc.* **1997**, *144*, 1609−1613.
(13) Nishimura, S. I.; Nakamura, M.; Natsui, R.; Yamada, A. *J. Am. Chem. Soc.* **2010**, *132*, 13596−13597.
(14) Tamaru, M.; Barpanda, P.; Yamada, Y.; Nishimura, S. I.; Yamada, A. *J. Mater. Chem.* **2012**, *22*, 24526−24529.
(15) Kim, H.; Lee, S.; Park, Y. U.; Kim, H.; Kim, J.; Jeon, S.; Kang, K. *Chem. Mater.* **2011**, *23*, 3930−3937.
(16) Uebou, Y.; Okada, S.; Egashira, M.; Yamaki, J. *Solid State Ionics* **2002**, *148*, 323−328.

(17) Palomares, V.; Serras, P.; Villaluenga, I.; Hueso, K. B.; Gonzalez, J. C.; Rojo, T. *Energy Environ. Sci.* **2012**, *5*, 5884−5901.
(18) Barpanda, P.; Ye, T.; Nishimura, S. I.; Chung, S. C.; Yamada, Y.; Okubo, M.; Zhou, H.; Yamada, A. *Electrochem. Commun.* **2012**, *24*, 116−119.
(19) Barpanda, P.; Yamada, A. Jpn. Patent JP 2011-193073, 2011.
(20) Hagemann, I. S.; Khalifah, P. G.; Ramirez, A. P.; Cava, R. J. *Phys. Rev. B* **2000**, *62*, R771−R774.
(21) Erragh, F.; Boukhari, A.; Elouadi, B.; Holt, E. M. *J. Crystallogr. Spectrosc. Res.* **1991**, *21*, 321−326.
(22) Sanz, F.; Parada, C.; Rojo, J. M.; Ruiz-Valero, C.; Saez-Puche, R. *J. Solid State Chem.* **1999**, *145*, 604−611.
(23) Beaury, L.; Derouet, J.; Binet, L.; Sanz, F.; Ruiz-Valero, C. *J. Solid State Chem.* **2004**, *177*, 1437−1443.
(24) Rietveld, H. M. *J. Appl. Crystallogr.* **1969**, *2*, 65−71.
(25) Rodriguez-Carvajal, J. *Physica B* **1993**, *192*, 55−69.
(26) Campbell, B. J.; Stokes, H. T.; Tanner, D. E.; Hatch, D. M. *J. Appl. Crystallogr.* **2006**, *39*, 607−614.
(27) Sengupta, P.; Sandvik, A. W.; Singh, R. R. P. *Phys. Rev. B* **2003**, *68*, 094423.
(28) Joshua, S. J. *Physica A* **1998**, *261*, 135−142.
(29) Whangbo, M. W.; Koo, H. J.; Dai, D. *J. Solid State Chem.* **2003**, *176*, 417−481.
(30) Momma, K.; Izumi, F. *J. Appl. Crystallogr.* **2011**, *13*, 1272−1276.